154

Tropical extratropical interaction associated with the 30-60 day oscillation and its impact on medium and extended range predictability

L. Ferranti, T.N. Palmer, F. Molteni and E. Klinker

Research Department

ABSTRACT

An observational and modelling study is made of tropical/extratropical interactions on timescales relevant to medium and extended range forecasting. Firstly an empirical orthogonal function analysis (EOF) is made of outgoing longwave radiation (OLR) in the tropics over the last 7 winters. Having removed the seasonal cycle and interannual variability, the principal EOFs describe the 30-60 day oscillation. A composite of extratropical 500mb geopotential height correlated simultaneously with this mode of tropical variability is constructed. In its two phase-quadrature components, this composite has significant projection onto the Pacific/North American teleconnection pattern, and onto the North Atlantic Oscillation pattern respectively.

The 500mb height composite is compared with the Simmons, Wallace and Branstator (SWB) mode of barotropic instability, which has similar periodicitiy, and similar spatial structure in both its phase-quadrature components. The adjoint SWB mode is also shown. This has most of its amplitude over Indonesia and the Indian Ocean. It is shown that a vorticity forcing derived from the EOFs of OLR project well onto this adjoint mode, and therefore can strongly excite the SWB mode. This is confirmed in a barotropic model integration, which is forced using the observed EOFs of OLR. The model response in the extratropics compares well with the observed composite oscillation in 500mb height.

In the final phase of this study, the ECMWF model has been integrated over four wintertime 20-day periods. For each period, five integrations have been performed; a control forecast, an integration in which the tropics are relaxed towards the verifying analysis, an integration in which the tropics are relaxed towards the initial analysis, an integration in which the extratropics are relaxed towards the verifying analysis, and finally an integration in which the extratropics are relaxed towards the initial analysis. The four initial dates were chosen on the basis that in the succeeding 20 days, observed OLR and extratropical height provided a reasonable realisation of each separate quarter of the composite oscillation.

It was found that in the extratropics, skill scores in the range of 11-20 days were noticeably improved, particularly over the Pacific (consistent with expectations from the data analysis). Indeed, maps showing the development in geopotential height from the first 5 days of the forecast were, in two cases, well correlated with the difference between the control integration and the integration with tropics relaxed to the verifying analysis.

Moreover, it was found that the systematic geopotential height error in the extratropics (ie the error averaged over the four experiments) was also significantly reduced when the forecasts in the tropics were relaxed towards the verifying analysis.

The impact of the extratropics on the tropics was also studied, where it was shown that the largest response was on the nondivergent component of the wind over the tropical east Pacific. Tropical skill scores and model systematic error in upper tropospheric streamfunction were significantly improved with the extratropics relaxed to the verifying analysis. By contrast, extratropical relaxation had a much smaller impact on the divergent component of the tropical wind.

1. Introduction

The extent to which tropical and extratropical atmospheric low-frequency variability interact has been the subject of keen interest in recent years. Much thinking in this area has been influenced by four seminal papers. Firstly, the so-called 30-60 day oscillation, detected by Madden and Julian (1971) from tropical station data, has been recognised as the principal mode of large-scale tropical intraseasonal variability. Secondly, the dominant teleconnection patterns between tropical diabatic heating anomalies and extratropical geopotential height were identified by Horel and Wallace (1981) and Wallace and Gutzler (1981) and interpreted in terms of Rossby wave dispersion theory by Hoskins and Karoly (1981).

However, with the development of numerical weather prediction (NWP) for the medium and extended range, the influence of the tropical circulations on forecasts of extratropical weather has also become an issue of great practical importance. Indeed, this paper was motivated by the need to quantify the degree to which forecast skill in the extratropics is influenced by model errors in the tropics, and conversely how tropical skill is influenced by the extratropics. A 'relaxation' technique, developed at ECMWF (Haseler, 1982; Klinker, 1989) gives some guidance on this question. Specifically, an NWP model is integrated in the usual manner, and compared with a second integration with identical initial conditions in which part of the model domain (the tropics, or the extratropics in this case) is forced towards the verifying analysis by adding a Newtonian relaxation term in the momentum and thermodynamic equations.

In the present paper, we consider cases in which we had prior expectation of strong tropical-extratropical interaction. Specifically we choose cases in circumstances when the 30-60 day oscillation was active in the tropics, and when significant transitions in extratropical weather regime occurred, characteristic of the composite teleconnection between tropical convective activity, and extratropical geopotential height.

This choice is guided by the results of an objective data analysis of large-scale low frequency variability of tropical outgoing longwave radiation (OLR), based on an empirical orthogonal function (EOF) analysis, and of extratropical 500mb geopotential height.

We present an interpretation of the results of the data analysis in terms of barotropic theory. Simmons Wallace and Branstator (1983) have identified a mode of barotropic instability with 45 day period, and a structure resembling our observed extratropical height composite associated with the tropical 30-60 day oscillation. We show maps of the adjoint of this mode, which gives the optimum structure to force the mode (Zhang, 1989; Farrell, 1989). This adjoint mode has most of its amplitude localised over

1

Indonesia and the Indian Ocean, and projects well onto the first two EOFs of (detrended) OLR determined by the data analysis. We show some integrations of the barotopic model using these two EOFs of OLR to provide a tropical vorticity forcing. The simulated extratropical response is clearly well correlated with the observed composite height pattern, both in its spatial pattern and its temporal variability.

2. Data Analysis

a. Data

Outgoing longwave radiation (OLR) is used as an indicator of large-scale vertical motion in the tropics (Arkin, 1984). The daily value of OLR used here is an average of twice daily measurements from polar orbiting scanning radiometers. The data were taken from 7 winters, each of 100 days, from 1 December 1980-10 March 1981 to 1 December 1986- 10 March 1987. The data were interpolated in time to fill small gaps in the first few years, and all values less than $60W/m^2$ were rejected. The data were spatially filtered using a projection onto spherical harmonics with a T21 truncation and transformed to a regular 5 x 5 degree latitude-longitude grid.

Northern Hemisphere 500 mb height data were taken from ECMWF archives, for the same period covered by the OLR data. The data were stored as projections onto a set of 23 empirical orthogonal functions (EOFs) which had been previously calculated from a much longer time series of 500mb height data (Molteni, 1987). These EOFs together explain 99% of the variance of the zonal mean of 5-day mean fields , and 87% of the variance of deviations about the zonal mean of 5-day mean fields. The EOF coefficients are used to characterise midlatitude flow in the northern hemisphere.

As our primary interest is in intraseasonal variability, both height and OLR data were filtered to remove interannual variability and the seasonal cycle. Specifically, for each winter, individually, each time series was detrended computing the deviations from a second order polynomial fitted by least squares. Our analysis of height and OLR data is performed on these deviation fields.

b. Analysis

Modes of low frequency variability of divergent flow were assumed to be representable by an EOF analysis of the detrended time series of OLR data. The first and second EOF patterns are shown in Fig. 1. Together these 2 EOFs explain 27% of the variance of 5-day mean. The main feature of these patterns are their large-scale coherent structure over the Indian Ocean, Indonesia and the equatorial central Pacific. The correlation between the coefficients $C_1(t)$, $C_2(t)$, of these two EOFs, for various time lags, is shown in Fig 2.

2

It can be seen that the maximum modulus of correlation exists with a lag/lead of about 12 days, suggesting that these two EOFs describe an oscillation in OLR with a period of about 48 days.

As has been found by earlier investigators (eg Lau and Chan, 1985), these patterns of OLR describe the well-known 30-60 day oscillation. This can be made more explicit by forming a four component composite of OLR by selecting those days when $C_2 > s_2$, $C_1 > s_1$, $C_2 < -s_2$, $C_1 < -s_1$. Here s_1 (s_2) denotes the standard deviation of the coefficient C_1 (C_2) respectively. These composite maps are shown in Fig 3. The main features of the divergent flow associated with the 30-60 day oscillation can be observed in these composites. The area of strong anomalous upper level divergence (negative OLR) over the Indian Ocean in Fig 3a, intensifies as it propagates toward Indonesia and New Guinea (Fig 3b and 3c). Finally (Fig 3d) there is a minimum in OLR to the east of the Phillipines, with the region of anomalous divergence sloping eastwards over the South Pacific. The speed of propagation is about 3-4m/s.

In order to demonstrate the apparent eastward propagation of this composite oscillation, time-lagged composite maps were formed from the OLR data. These are shown in Fig. 4. Each time-lagged composite is an average of the fields that occurred 12 days later than the fields included in one of the synchronous composite shown in Fig. 3. So, for example, the pattern shown in Fig 4b is a composite of those fields which occurred 12 days after those forming the (synchronous) composite in Fig 3a. If we had a perfect 48 day cycle, figures 3 and 4 should be identical. Overall, the resulting shifted composite bears many similarities to the original. In detail, there are some differences, however. In particular, the 12-day shifted composite from data in Fig 4a does not show the strong negative centre over the Indian ocean. This suggests that the oscillation itself originates in this area. Moreover, the composite in Fig 4d does not show a maximum in the northern tropics to the east of the Phillipines as the synchronous counterpart in Fig 3d does. It is clear, therefore, that part but not all of the variability in C_1 and C_2 can be described by a purely periodic 48-day oscillation.

We now illustrate coherent fluctuations in the extratropical geopotential height field which may be associated with these modes of tropical low-frequency variability. Fig 5 shows composite patterns of extratropical 500mb height anomaly synchronous with the data comprising the OLR composites in Fig 3. That is to say, in Fig 5, each map is an average of geopotential height anomaly constructed according to whether, for each day, $C_2 > s_2$, $C_1 > s_1$, $C_2 < -s_2$, or $C_1 < -s_1$.

3

An indication of a coherent extratropical cycle in geopotential height is shown by the relationship between composites with opposite phases. Features with opposite sign in Fig 5 correspond to opposite phases in the OLR cycle. The pattern of geopotential height defined when the $C_1 > s_1$ (Fig 5b) and $C_1 < -s_1$ (Fig 5d) clearly projects onto the Pacific/ North American (PNA) mode (Wallace and Gutzler, 1981) of low-frequency variability. Hence, from Figs 5b and 5d, we would associate the phase of the OLR composite cycle in which convective activity to the east of the Phillipines is enhanced, with positive PNA index with conventional notation. The pattern of geopotential height defined when $C_2 > s_2$ (Fig 5a) and $C_2 < -s_2$ (Fig 5c) is clearly global in extent, but projects significantly onto the North Atlantic Oscillation (NAO, Wallace and Gutzler, 1981). With conventional notation, we would associate Fig 5c with positive NAO index. .

The magnitude of the composite height anomalies should be compared with climatological estimates of low frequency variability in the extratropics. Over the north Pacific, the amplitude of the height anomaly during the PNA phase of the oscillation is about 6-7 dam. By comparison, climatological values of low-pass variability in 500mb height over this region are about 12dam, as given by Lau et al (1981). Hence, over the north Pacific, the height composite associated with tropical low-frequency variability explains only up to about 25% of the total variance. We shall see (section 4) that this estimate is consistent with the degree of improvement in forecast skill of extended range forecasts in which the tropics have been relaxed towards the verifying analysis.

Time-lagged composite maps of geopotential height (Fig. 6), constructed with a shift of 12 days relative to the days used in the Fig. 5 composites, indicate an oscillation in phase with the OLR composites. The lagged composite in Fig 6a (formed from fields which occur 12 days later than the corresponding field in the synchronous composite in Fig 5d) is very similar to the synchronous composite in Fig 5a, indicating a clear transition from postive PNA to negative NAO. Similarly the transitions from negative NAO to negative PNA, and from negative PNA to positive NAO are reasonably clear cut. Only the transition from negative NAO to positive PNA is not clearly shown in the lagged composite in Fig 6d.

This discrepancy is consistent with the absence of a negative centre in OLR to the east of the Phillipines in the lagged composite in Fig 4d. In fact, it appears that this centre of convention is important for the excitation of a positive PNA pattern.

This can be made clear by showing synchronous and 5-day time-lagged maps of the correlation between OLR averaged between 15-20N, 135-150E (close to the maximum negative OLR in Fig 3d) and geopotential height. (A similar analysis has been made by

Liebmann and Hartmann, 1984). With synchronous correlation between OLR and height (Fig 7a), the three largest teleconnection coefficients occur at the centres of action of the PNA pattern. When geopotential height lags OLR by 5 days (Fig 7b) the magnitude of the correlations are somewhat reduced, though again the largest values occur at the centres of action of the PNA pattern. When geopotential height leads OLR by 5 days (Fig 7c), a rather different pattern emerges, with two teleconnection maxima occuring over the extratropical Asian land mass and west Pacific, suggestive of a wavetrain propagating equatorward towards the tropical west Pacific].

In conclusion, we have analysed OLR and height data, and found a 48-day periodicity in the first 2 EOFs of OLR which correlates with the PNA and NAO modes of the extratropical flow. We shall use this analysis to choose, in section 4, four 20-day periods when the extratropical flow was undergoing a transition between these modes.

3. Tropical- extratropical interaction in a barotropic model

In this section we speculate on theoretical reasons for the observed teleconnections between the tropical 30-60 day mode as revealed by the OLR composites in Figs 3, 4, and the composite extratropical 500mb height anomalies shown in Figs 5, 6. Although some results of our data analysis (see also Liebmann and Hartmann, 1984) and of the numerical experiments described in the next section suggest that the tropical circulation is not totally independent of the midlatitude flow, we shall concentrate here on one aspect of tropical-extratropical interaction, namely the influence of anomalous divergent flow in the tropics on the midlatitude circulation.

In the work of Hoskins and Karoly (1981), the barotropic vorticity equation was linearised about a zonally symmetric basic state. As a potentially straight forward extension to this, Frederiksen (1986) and Simmons (1982) considered solutions linearised about a zonally varying basic state. In Simmons' work the basic state was taken from the climatological 300mb flow. Simmons' findings can be summarised using the schematic diagram from Simmons et al (1983), shown here in Fig 8. This diagram shows that the long-term response to a localized forcing is maximised in the extratropical jet exit regions over the Pacific. Moreover, this maximum response can be most strongly excited by forcing over the tropical west Pacific, Indonesia and the Indian Ocean. (A secondary maximum over the north Atlantic associated with forcing over the Caribbean is also found.) In Simmons et al's integrations, perturbation energy is extracted from the basic state flow through barotropic energy conversions associated with both the meridional and zonal gradients of the basic state wind, the latter being particularly strong in the jet exit regions.

From Fig 8 it can be seen that the tropical vorticity forcing necessary to excite a given north Pacific response changes sign from the west Pacific to the Indian ocean. Superimposed on the figure are contours of the observed first EOF of OLR (from Fig 1) which is associated with the PNA phase of the extratropical oscillation. It can be seen that there is a remarkable correspondence between the contours of the observed EOF and the regions of plus and minus forcing from the barotropic model. The correspondence is more marked if the EOF is multiplied by the Coriolis parameter to give a vorticity forcing.

Further analysis of these barotropic model solutions was given in Simmons et al (1983), where the most unstable normal mode of the linearised vorticity equation was calculated (hereafter the SWB mode). The eigenvalue of this mode gave an e-folding time of less than 7 days with a period of 45 days. The mode is shown in Fig 9 for two realisations in (temporal) phase quadrature. It can be seen that in one phase, the mode projects significantly onto the NAO mode; in the other phase it projects onto the PNA mode. Hence, it is clear that this mode projects significantly onto the observed four-component (48-day period) composite shown in Fig 5.

From a theoretical point of view, let us consider the question of how to optimally excite the SWB mode with a vorticity forcing $F(x,y)$. Writing the linearised vorticity equation as

$$L \psi = F \tag{1}$$

(where ψ is streamfunction) and expanding F in terms of eigenfunctions E_j of the linearised vorticity operator L

$$F = \sum_j f_j E_j \tag{2}$$

we have

$$\psi = \sum_j \frac{f_j}{\sigma_j} E_j \tag{3}$$

where σ_j are the eigenvalues of L and

$$f_j = <E_j^* F> \tag{4}$$

Here E_j^* are the eigenvectors of the adjoint operator L^* (Branstator, 1986; Zhang, 1989), which satisfy the biorthogonality relation

6

$$\langle E_i^*, E_j \rangle = \delta_{ij} \tag{5}$$

Here $\langle ..,.. \rangle$ is the barotropic energy inner product. The eigenvalue associated with the jth adjoint eigenvector is the complex conjugate of the eigenvalue associated with the jth eigenvector. With the zonally-varying sheared January basic state flow, L is not self adjoint.

From 1-5 it can be seen that in order to optimally excite the dominant eigemode E_1, the forcing F should project onto the adjoint mode E_1^*. Fig 10 shows the two phases of the first adjoint eigenvector (in phase quadrature) over the west Pacific, Indonesia and the Indian Ocean, where its amplitude is concentrated. Since the period is identical to that of the original SWB mode, the two phases shown in Fig 10 describe an oscillation with a period of 48 days. It is clear that a vorticity forcing constructed from the two EOFs of OLR shown in Fig 1, will project significantly onto this adjoint mode, and therefore strongly excite the SWB mode in the extratropics.

In order to demonstrate this explicitly, we have integrated a barotropic model using these observed EOFs of OLR to provide a tropical vorticity forcing. The model is a little more complicated than the purely nondivergent barotropic model used by Simmons et al (1983). In particular, we include both the vortex compression effect of orography h, and introduce a Rossby radius of deformation R. The model equation of motion is given by (Pedlosky, 1979)

$$\frac{\partial}{\partial t} (\nabla^2 - R^{-2}) \psi = T(\psi) + F_0 + F'(t) \tag{6}$$

where

$$T(\psi) = -V_\psi \cdot \nabla (\nabla^2 \psi + f(1 + \frac{h}{h_0})) - \frac{1}{\tau} \nabla^2 \psi \tag{7}$$

$$F_0 = T(\psi_0) \tag{8}$$

$$F'(t) = - (f + \nabla^2 \psi_0) D(t) - V_\chi(t) \frac{\partial}{\partial y} (f + \nabla^2 \psi_0) \tag{9}$$

$$D(t) = a[\sin(\omega t) E_1 + \cos(\omega t) E_2] \tag{10}$$

In Eqs. 8 and 9 ψ_0 is a background streamfunction, equal to a 300mb January climatological flow. The (artificial) forcing F_0 is applied to make ψ_0 a steady solution of the vorticity equation (in absence of the 30-60 day oscillation). The dissipation time τ is assumed to be 10 days.

For the anomalous forcing F'(t) we assume that the OLR field is proportional to upper level convergence, with a constant of proportionality derived from a regression equation between OLR and ECMWF analysed 300mb divergence. The total divergence field is computed as a linear combination of the first 2 OLR EOFs E_1 and E_2 in Eq. 5; the coefficients vary in time with a period of 48 days ($\omega = 2\pi/48$ d). The root-mean-square amplitude of the divergence field (a in Eq. 10) is set to $.4 \cdot 10^{-6} s^{-1}$.

The vorticity forcing F' provided by the OLR EOFs includes the term describing the meridional advection of total vorticity by the divergent wind (Sardeshmukh and Hoskins, 1987). (If this term is not included, the extratropical response is phase shifted because the effect of the first term on the right hand side of (9) underestimates the equatorial forcing and amplifies the subtropical forcing). The actual fields of F' so derived are shown (in phase quadrature) in Fig 11.

The barotropic model was integrated for 9x48=432 days, with the initial vorticity forcing given by the field in Fig 11a. The streamfunction response to the forcing, averaged over the last 8 cycles of the forcing is shown in Fig 12 a-g. In this figure, the streamfunction has been multiplied by the Coriolis parameter to give an equivalent geopotential field. The diagram is organised so that each map shows a composite over a 6 day period. Fig 12 a corresponds to a maximum in C_2, Fig 12 c corresponds to a maximum in C_1, Fig 12 e corresponds to a minimum in C_2, and Fig 12 g corresponds to a minimum in C_1.

There is manifestly some resemblence between the simulated response in Fig 12 and the observed cycle in Fig 3. The negative (positive) phase of the NAO mode is clearly seen in Fig 12h (d). The positive (negative) phase of the PNA mode is shown in Fig 12b (f). Note that the phase relation of the model response is close to that observed in Fig 5. However, the resemblence between the observed and simulated cycles is only approximate. Indeed the response in our barotropic model is sensitive to the orographic specification, to the value of the Rossby radius of deformation, to the formulation of divergence forcing, and to the basic state flow.

8

4. Relaxation experiments

a. Cases chosen

As mentioned in the introduction, the principal motivation for this study is to assess the degree to which forecast skill in the extratropics is influenced by model errors in the tropics, and conversely how tropical skill is influenced by the extratropics. From the diagnostic study above, we choose periods in which it would appear that tropical extratropical interaction is strong. If the 30-60 day oscillation is indeed a global-scale mode, then we can expect that in cases where extratropical forecast skill is strongly influenced by the tropical flow, the tropical flow will be similarly influenced by the extratropical skill.

We choose three 20-day periods from the winter 1984/85 and one 20-day period from the winter 1985/86. Together they describe approximately each phase of the transition in extratropical height associated with the 30-60 day oscillation. The 500mb height fields for days 1-5 averaged and days 11-15 averaged, for each of the 4 periods are shown in Fig 13. Time series of the coefficients of the first 2 EOFs of OLR for these two winters are shown in Fig 14. For the first case (initial date 4 December 1984), it can be seen that from days 1-5 to 11-15, the extratropical flow evolves towards negative PNA index, approximately describing the transition from Fig 5a to Fig 5b. The 5-day mean values of the coefficients (C_1, C_2) evolved from (2.4, 3.2) to (5.4, -3.1), ie C_1 increasing, C_2 decreasing. The 500mb height field for the second case (initial date 25 December 1984) evolved from negative to positive PNA index, approximately describing the transition from Fig 5b to Fig 5d. The 5-day mean values of the coefficients (C_1, C_2) evolved from (-4.1, -2.9) to (-7.8, -1.6), ie C_1 decreasing, C_2 increasing. The 500mb height field for the third case (initial date 22 January 1985) evolved from positive PNA index, approximately describing the transition from Fig 5d to Fig 5a. The 5-day mean values of the coefficients (C_1, C_2) evolved from (-1.7, 3.2) to (6.3, 3.9), ie C_1 increasing, C_2 increasing. Finally, the 500mb height field for the fourth case (initial date 19 January 1986) evolved from positive NAO index, approximately describing the transition from Fig 5c to Fig 5d. In particular, during this episode, a particularly high amplitude block developed over Europe (Hoskins and Sardeshmukh, 1987). The 5-day mean values of the coefficients (C_1, C_2) evolved from (4.6, -5.9) to (-5.7, -1.0), ie C_1 decreasing, C_2 increasing.

Note that from Fig 5 the evolution of the coefficients of OLR between days 1-5 and 11-15 is broadly consistent with the composite evolution in OLR associated with the four respective transitions in geopotential height.

b. relaxation technique

For each 20 day period, five integrations were made. In the first control experiment, the ECMWF (cycle 30) model (see eg Simmons et al., 1989) was integrated at T42 resolution from the given intial date. The four additional integrations were made from the same initial date, but included the addition of a term

$$-\alpha(X-X^*)$$

in the model equations for vorticity, divergence and temperature. This term relaxes the model variable X towards some prescribed value X*. In the following, two choices for X* are made: the verifying analysis and the initial conditions. The value of α (the relaxation coefficient) is spatially dependent. In the tropical relaxation experiments (see Fig 15), it varied from a value of (8hr)$^{-1}$ between 15N-15S, decreasing to a value of 0 poleward of 25 degrees. In the extratropical relaxation experiments, it varied from a value of (8hr)$^{-1}$ between the poles and 35 degrees, decreasing to a value of 0 equatorward of 25 degrees.

Hence, relative to a control experiment, we are able to examine the impact in the extratropics of relaxing the tropics towards the analysis (perfect tropical prognosis) or towards the initial conditions (persistent tropics). The comparison between the two relaxation experiments allows us to evaluate the influence of tropical variability on extratropical variability. Similarly we are able to examine the impact in the tropics of relaxing the extratropics towards the analysis (perfect extratropical prognosis) or towards the initial conditions (persistent extratropics).

c. composite results

First we show diagrams giving forecast skill scores averaged over the four cases. We used three verification areas, each 120 degrees of longitude in extent: the "Atlantic" (90W-30E), "Asia" (30E-150E) and the "Pacific" (150E-90W). For the tropical relaxation experiments, the verification is performed within latitudes (30N-90N). For the extratropical relaxation experiments, the verification is performed within latitudes (20N-20S). The verification is performed only on fields truncated to T15.

In order to compare directly scores in the tropics and extratropics, it was decided to verify the forecasts in terms of anomaly correlation coefficient of 5-day mean 200mb vorticity (and in addition, in the tropics, 200mb divergence). These scores are shown in Fig 16, averaged over all four experiments. The left hand column shows extratropical vorticity scores; the middle column shows tropical vorticity scores; the right hand column shows tropical divergence scores. Scores for the control forecast are shown as solid lines; scores for the experiments with relaxation towards the analysis are shown as

10

dotted lines; scores for the experiments with relaxation towards initial conditions are shown as dashed lines.

From the left hand column, it can be seen that the biggest impact of tropical relaxation is in the Pacific region. Beyond day 10, the anomaly correlation coefficient in this region is about 0.3 for the control integration. With the tropics relaxed to the verifying analyses, the extratropical Pacific scores increase to about 0.5. With the tropics relaxed to the initial analysis, the Pacific scores decrease to about 0.1. It is interesting to note that the increase in percentage of variance explained between the relaxation to verifying analysis and relaxation to initial conditions is about the same as the percentage of variance explained by the 500mb height composite in Fig 5 during the PNA phase of the oscillation, as a fraction of Lau et al's (1981) estimate of climatological variance (about 25%).

On average, the impact of relaxation over the extratropical Asian region is less pronounced than over the Pacific, and the impact of relaxation over the Atlantic appears to be smallest of all three areas. The relatively large impact over the Pacific region is to be expected, both from the observational data analysis, and from the results of Simmons et al (1983).

In the tropics, it can be seen from the centre and right hand columns that the impact of relaxation in midlatitudes is more pronounced on the nondivergent flow than on the divergent flow. As far as the regions are concerned, the impact of relaxation on 200mb vorticity scores is equally large in the tropical Pacific and Asian regions, and it is at least as strong as the impact in northern extratropics. One should also note that (with the exception of the tropical divergent flow in the Asian sector) forecasts with relaxation to the initial conditions are consistently less skilful than control forecasts, which is a further indication of a reciprocal interaction between tropical and extratropical low-frequency variability.

Fig 17 shows the impact of tropical relaxation on 'systematic error' in extratropical 500mb height. The control 'systematic error' is defined as the average error from days 11-20 over the four experiments and is shown in Fig 17a. It can be seen that there are two major negative centres over the north Pacific and north Atlantic, and positive height errors over north America, Europe and east Asia.

The day 11-20 extratropical systematic error in the experiments with the tropics relaxed to the verifying analysis is shown in Fig 17b. There is a large reduction in the magnitude of the negative north Pacific centre from 167m to 97m. Similarly, the

systematic error over north America is also reduced. Over the Euro/Atlantic region, there is a marked reduction in the magnitude of the negative height anomaly over the north east Atlantic, but an increase in the positive height anomaly over Europe. As a result, the gradient in height error over the UK is not substantially reduced. This result, as well as the occasional decrease of skill scores over the Euro/Atlantic observed in some tropical relaxation experiments, suggests that over this region, extratropical errors might be locally compensated by tropical errors. Overall, however, it can be seen that with perfect tropical prognosis, the model extratropical systematic error can be reduced substantially on a time scale of 10 to 20 days.

The impact in the tropics of relaxation to the extratropical analysis can be seen in Fig 18 for 200mb streamfunction, and in Fig 19 for 200mb velocity potential. Consistent with the scores, the largest impact is on the nondivergent flow, where systematic errors over the east Pacific are significantly reduced. By contrast, the impact of extratropical relaxation on systematic error in velocity potential is much weaker.

d.   individual cases of tropical relaxation

We show in Fig 20, maps of 500mb height for day 16-20 of the control integration (left column), the integration with relaxed tropics (middle column), and the verifying analysis (right column), for each individual case. For brevity, forecast maps of 500mb height for earlier times will not be shown, though the verifying analysis for days 1-5 and 11-15 were shown in Fig 13.

The verifying analysis for the 4 December 1984 case (first row) shows a split flow over eastern Europe (which had developed from a strong ridge in the preceding pentad) and a weak, broad ridge over the Pacific, indicating an elongated wavenumber two pattern to the flow overall. The control integration is clearly poor in all respects. The relaxed integration, on the other hand, has captured approximately the split European flow, and the positive height centre near 60E, 50N is simulated accurately. There is a weak ridge over the mid-Pacific, though its strength and position is not accurately reproduced.

The analysis for the 25 December 1984 case (second row) shows a northeast-southwest oriented ridge over the east Atlantic and the west coast of Europe with a cut-off low over eastern Europe. The control integration has weak counterparts to these features. However, in the relaxed integration, they are both strongly enhanced. Indeed, over the British Isles, the relaxed experiment has developed a isolated maximum in geopotential height.

The analysis for the 22 January 1985 case is shown in the third row. The ridge over the Atlantic in the previous pentad has strongly weakened and the ridge over the Gulf of Alaska in the previous pentad has been replaced by a trough. In the relaxed experiment, the east Atlantic ridge is fairly strong, and the mid-Pacific ridge is too weak. However the trough over the Gulf of Alaska is well simulated, and overall the flow is clearly superior to the control simulation.

The analysis for the 19 January 1986 case (fourth row) shows the intense dipole blocking discussed by Hoskins and Sardeshmukh (1986) and Brankovic et al (1989). Note also the strong ridge over the northeast Pacific. The European block is utterly missed in the control integration, but a significant ridge has developed in the relaxed experiment. Note also the cut-off low over southern Europe. Over the Pacific it can be seen that the relaxed experiment has simulated the strong ridge well, compared with the control integration.

Only in one of the four integrations (22 January) did we see a significant impact of tropical relaxation with respect to the control forecast in the range of days 6-10. However, for this case the EOF coefficients of OLR had very large variations between days 1 to 10, and Fig 21 shows that there was a clear beneficial impact of tropical relaxation on the flow over the north Pacific.

Although the parametrization of tropical convection activity used in cycle 30 of the ECMWF model is far from being totally satisfactory, we should not assume that the tropical fields simulated in the control experiment are completely wrong, especially of day 6-10. A clearer impression of the influence of tropical variability on extratropical variability can be gained by comparing forecasts with relaxation to the initial data in the tropics, forecasts with relaxation to actual data in the tropics, and the observed flow.

For example, for the experiment started on 22 January 1985, we show (Fig 22) maps of the difference between experiments with relaxation to verifying analysis and relaxation to initial analysis (top row) and of the difference between the each 5-day mean analysis field and days 1-5 of the analysis (bottom row). It can be seen that even for days 6-10, the difference between the two relaxation experiments correlates positively with the observed tendency between the first and successive five day mean field. This indicates that the representation of tropical variability is (at least in some cases) an important factor for a realistic prediction of transitions between extratropical flow regimes.

CONCLUSIONS

Not many years ago, the domain of integration in most numerical weather prediction models did not include the tropics. As computational power increased, and as prediction progressed towards the medium range, it was recognised that there were occasions when the tropics had a measurable influence on the development of extratropical weather, and global models were developed. In this paper we have attempted to show that, in addition, for prediction beyond the medium range, the impact of the tropics on the extratropics is typically, rather than occasionally, large.

The technique we have used to examine the impact of the tropics on the extratropics in an NWP model was through a relaxation of model fields to the verifying analysis, or initial analysis. However, the cases were chosen to occur during periods when the 30-60 day oscillation was active. These periods were identified by first performing a diagnostic analysis using observed fields of tropical OLR and extratropical geopotential height. We attempted to explain our results using barotropic theory, and idealised integrations of a barotropic model.

Parallel experiments were also run, in which extratropical fields were relaxed towards observed data, and a noticeable improvement was found on skill scores for the forecast tropical flow, in particular for its rotational component. These results are suggestive of a clear, reciprocal interaction between tropical and extratropical low-frequency variability.

We conclude by stating that skilful prediction of the large-scale tropical flow is a prerequisite for extratropical extended-range prediction. Since tropical systematic errors in many NWP models are still quite sizeable (see Palmer et al., 1989), there is a requirement for considerable model improvement before extended range forecasting can be considered viable.

14

References

Arkin, P. A., 1984: An examination of the southern oscillation in the upper tropospheric tropical and subtropical wind field. Ph. D. dissertation, University of Maryland, 240pp.

Brankovic, C., T.N. Palmer, F. Molteni, S. Tibaldi and U. Cubasch, 1989: Extended-range predictions with ECMWF models: III A study with time-lagged ensembles. Submitted to Q.J.R.Meteor.Soc.

Branstator, G. 1985a: Analysis of general circulation model sea surface temperature anomaly simulations using a linear model. Part I: forced solutions. J. Atmos. Sci., 42, 2225-2241.

Branstator, G. 1985b: Analysis of general circulation model sea surface temperature anomaly simulations using a linear model. Part II: Eigenanalysis. J. Atmos Sci., 42, 2242-2254.

Farrell, B., 1989: Optimal excitation of baroclinic waves. J.Atmos.Soc., 46, 1193-1206.

Frederiksen, J. S., 1986: Instability theory and nonlinear evolution of blocks and mature anomalies. Adv. in Geophys., 29, 277-304.

Haseler, J., 1982: An investigation of the impact at middle and high latitudes of tropical forecast errors. ECMWF Tech. Rep. No. 31

Horel, J. D. and Wallace, J. M., 1981: Planetary scale atmospheric phenomena associated with the Southern Oscillation. Mon. Wea. Rev., 109, 2080-2092.

Hoskins, B. J. and Karoly, D., 1981: The steady linear response of a spherical atmosphere to thermal and orographic forcing. J. Atmos Sci., 38, 179-1196.

Hoskins B. J. and P.D. Sardeshmukh, 1987: A diagnostic study of the dynamics of the northern hemisphere winter of 1985-86. Quart. J. R. Met. Soc., 113, 759-778.

Klinker, E., 1989: Investigation of systematic errors by relaxation experiments. Submitted to Quart. J. Roy. Met. Soc.

Lau, K.-M. and Chan, P.H., 1985: Aspects of the 40-50 day oscillation during the Northern Winter as inferred from Outgoing Longwave Radiation. Mon.Wea.Rev., 113, 1889-1909.

Lau, K.-M. and T. J. Phillips, 1986: Coherent fluctuations of extratropical geopotential height and tropical convection in intraseasonal timescales. J. Atmos. Sci. 43, 1164-1181.

Lau, N-C., White, G.M. and Jenne, R.L. 1981: Circulation statistics for the extratropical northern hemisphere, based on NMC analyses. NCAR Tech. Note TN-171-STR, NCAR, Boulder, Colorado.

Liebmann B. and D. L. Hartmann, 1984: An observational study of tropical-midlatitude interaction on intraseasonal timescales during winter. J. Atmos. Sci., 41, 3333-3350.

Livezey, R. E. and Mo, K. C., 1988: Tropical-extratropical teleconnections during the northern hemisphere winter. Part II: Relationships between monthly mean northern hemisphere circulation patterns and proxys for tropical convection. Mon. Wea. Rev.

Madden, R. A. and Julian P.R., 1971: Detection of a 40-50 day oscillation in the zonal wind in the tropical Pacific. J. Atmos. Sci., 28, 707-708.

Matsuno, T. and I. Hirota, 1966: On the dynamical stability of polar vortex in wintertime. J. Met. Soc. Japan., 44, 122-128.

Molteni, F., 1987: Empirical Orthogonal Function Analysis of the zonal and eddy components of 500mb height fields in the northern extratropics. ECMWF Technical Report. No. 61.

Palmer, T. N., 1988: Medium and extended range predictability, and stability of the PNA mode. Quart. J. R. Met. Soc., 114, 691-713.

Palmer T. N. and D. A. Mansfield, 1986a: A study of wintertime circulation anomalies during past El Nino events using a high resolution general circulation model. I: Influence of model climatology . Quart J. R. Met. Soc., 112, 613-638.

Palmer T. N. and D. A. Mansfield, 1986b: A study of wintertime circulation anomalies during past El Nino events using a high resolution general circulation model. II: Variability of the seasonal mean response. Quart J. R. Met. Soc., 112, 639-660.

Palmer, T.N., C. Brankovic, F. Molteni and S. Tibaldi, 1989: Extended-range predictions with models. I Interannual variability of operational model integrations. Submitted to Quart.J.R.Met.Soc.

Pedlosky, J., 1979: Geophysical Fluid Dynamics. Springer-Verlag.

Sardeshmukh P. D. and Hoskins B. J., 1988: On the generation of global rotational flow by steady idealised tropical divergence. J. Atmos. Sci., 45, 1228-1251.

Simmons, A. J., 1982: The forcing of stationary wave motion by tropical diabatic heating. Quart. J. R. Met. Soc., 108, 503-534.

Simmons, A. J., J. M. Wallace and G. W. Branstator, 1983: Barotropic wave propagation and instability, and atmospheric teleconnection patterns. J. Atmos. Sci., 40, 1363 1392.

Simmons, A.J., D.M. Burridge, M. Jarraud, C. Girard and W. Wergen, 1989: The ECMWF medium-range prediction models development of the numerical formulations and the impact of increased resolution. Meteorol.Atmos.Phys., 40, 28-60.

Wallace, J. M. and D. S. Gutzler, 1981: Teleconnections in the geopotential height field during the northern hemisphere winter, Mon. Wea. Rev., 109, 784-812.

Zhang, Z., 1989: PhD Thesis. Department of Meteorology, Reading University.
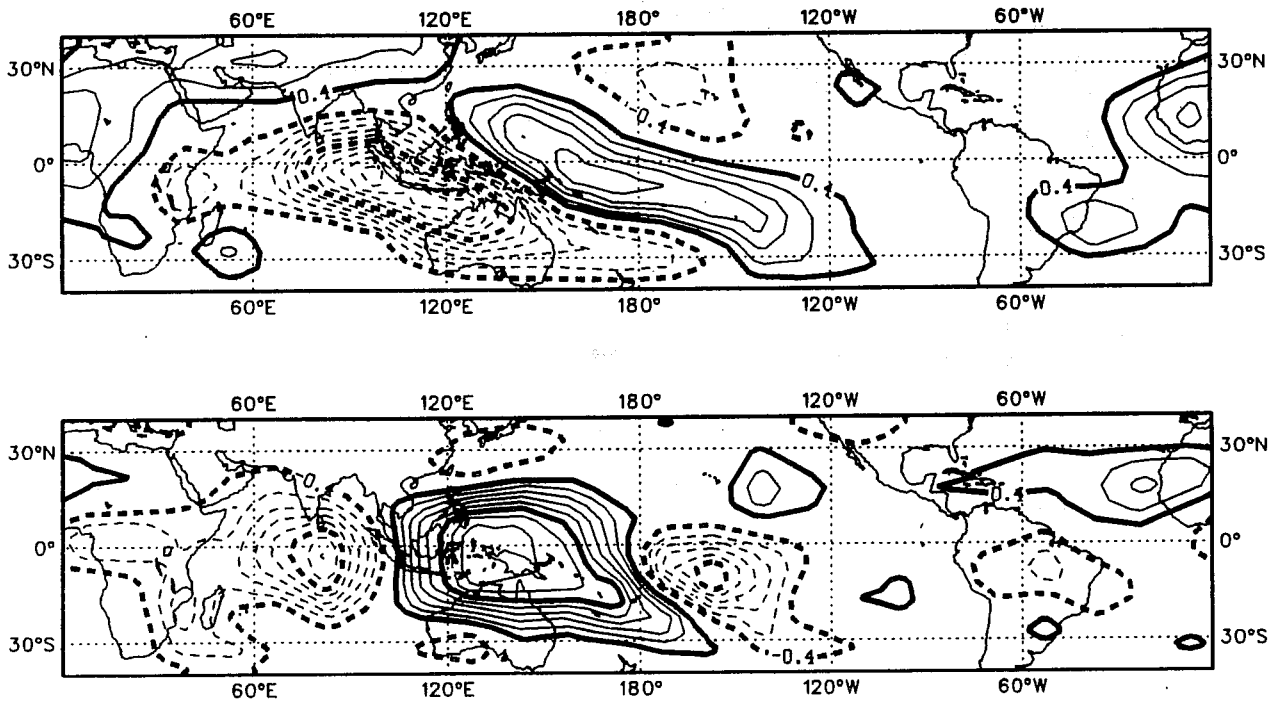
Fig. 1   First two EOFs derived from daily fields of tropical OLR for seven northern winters (1980-1987). Data has been detrended to remove interannual variability and the seasonal cycle. Contour interval .4.
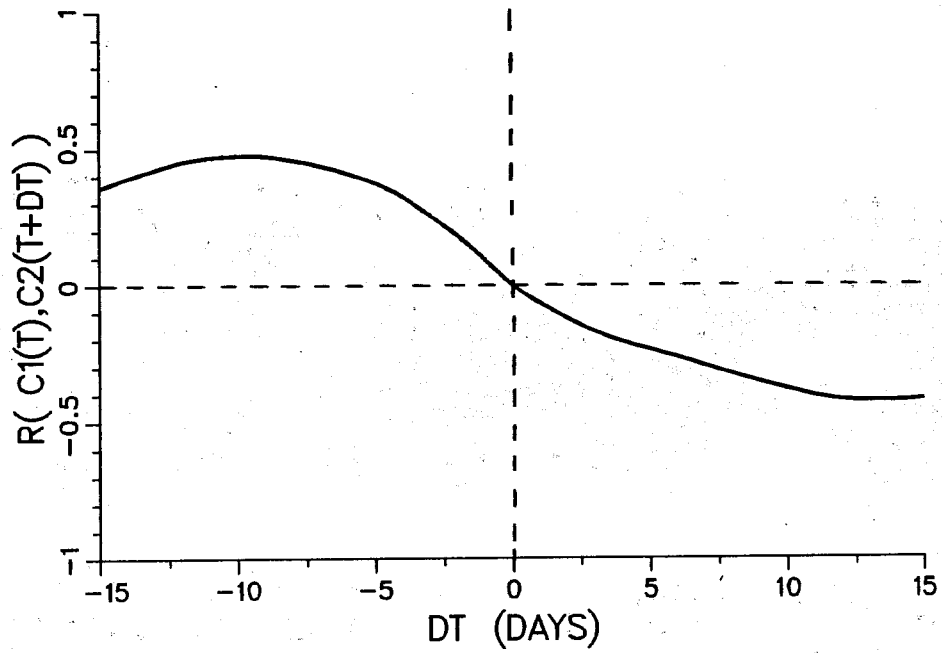
Fig. 2   Correlation between coefficents of first and second EOF of OLR using 700 winter values as a function of time lag in days.
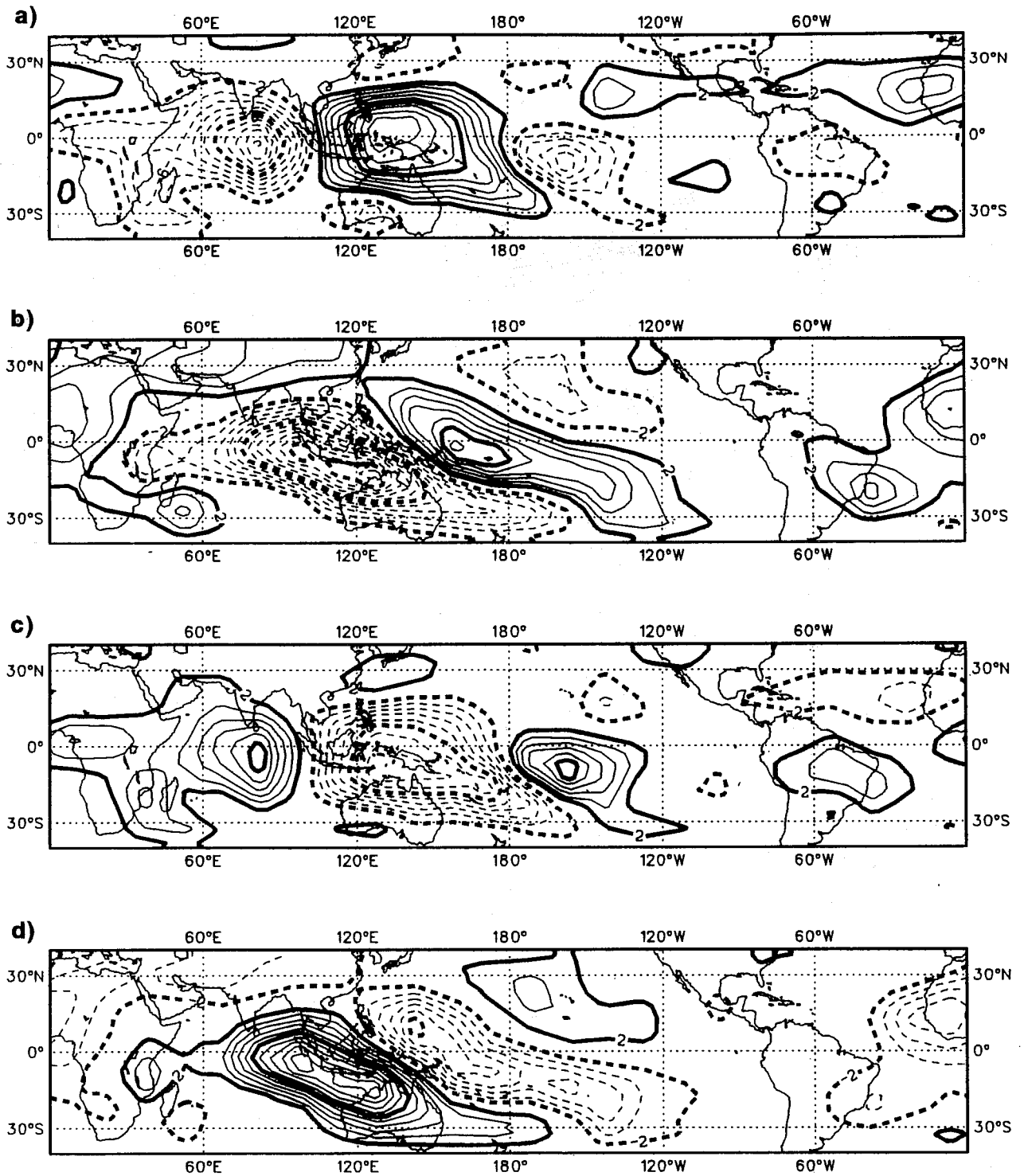
Fig. 3   Composite of OLR formed by taking from the 700 winter fields, days where a) the coefficient of the second EOF was greater than one standard deviation. b) the coefficient of the first EOF was greater than one standard deviation. c) the coefficient of the second EOF was less than minus one standard deviation. d) the coefficient of the first EOF was less than minus one standard deviation. Contour interval 2 W/m².
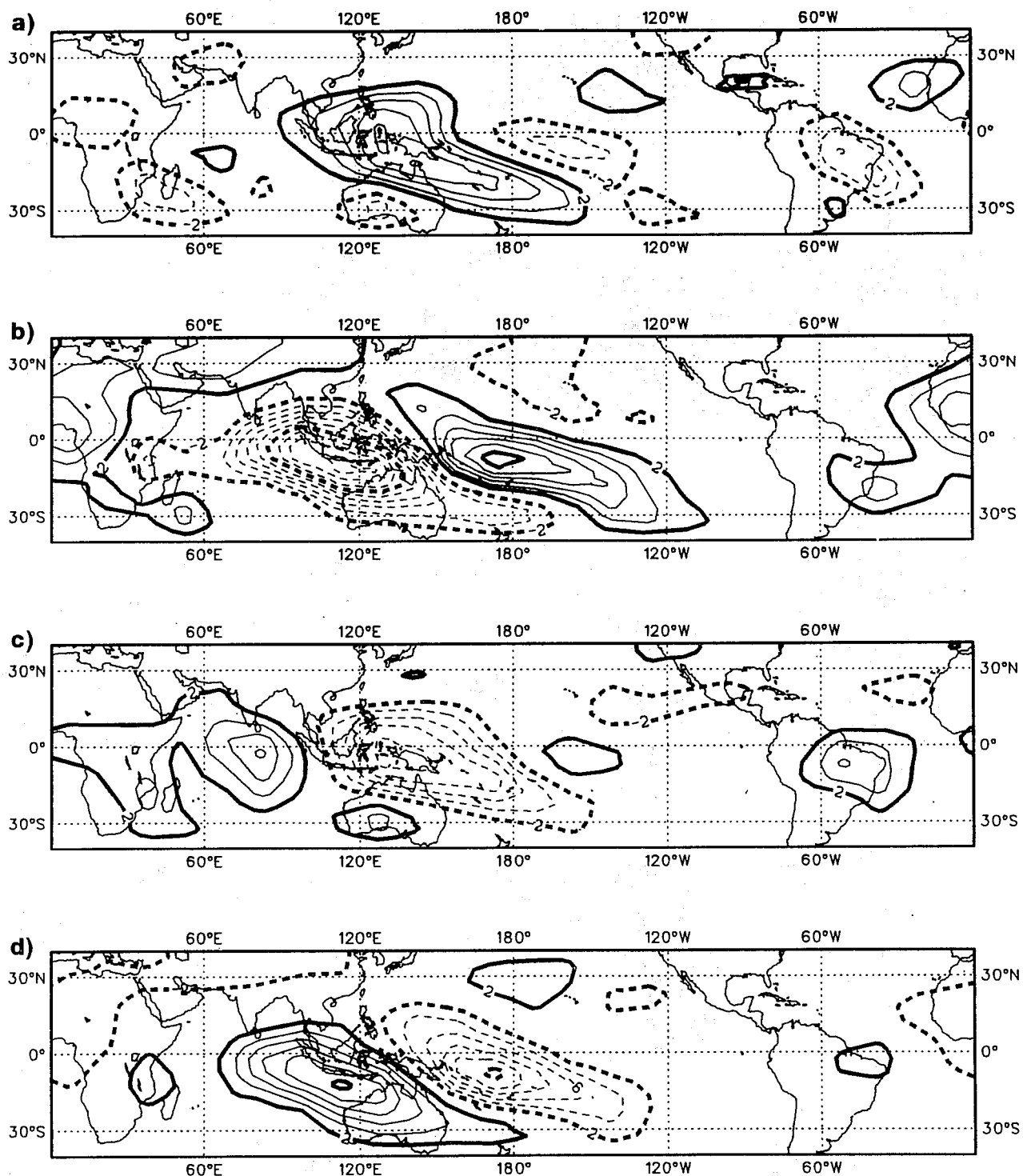
Fig. 4   Composite of OLR formed by taking from the 700 winter fields those days which are 12 days after a) the coefficient of the first EOF was less than minus one standard deviation. b) the coefficient of the second EOF was greater than one standard deviation. c) the coefficient of the first EOF was greater than one standard deviation. d) the coefficient of the second EOF was less than minus one standard deviation. Contour interval 2 W/m².
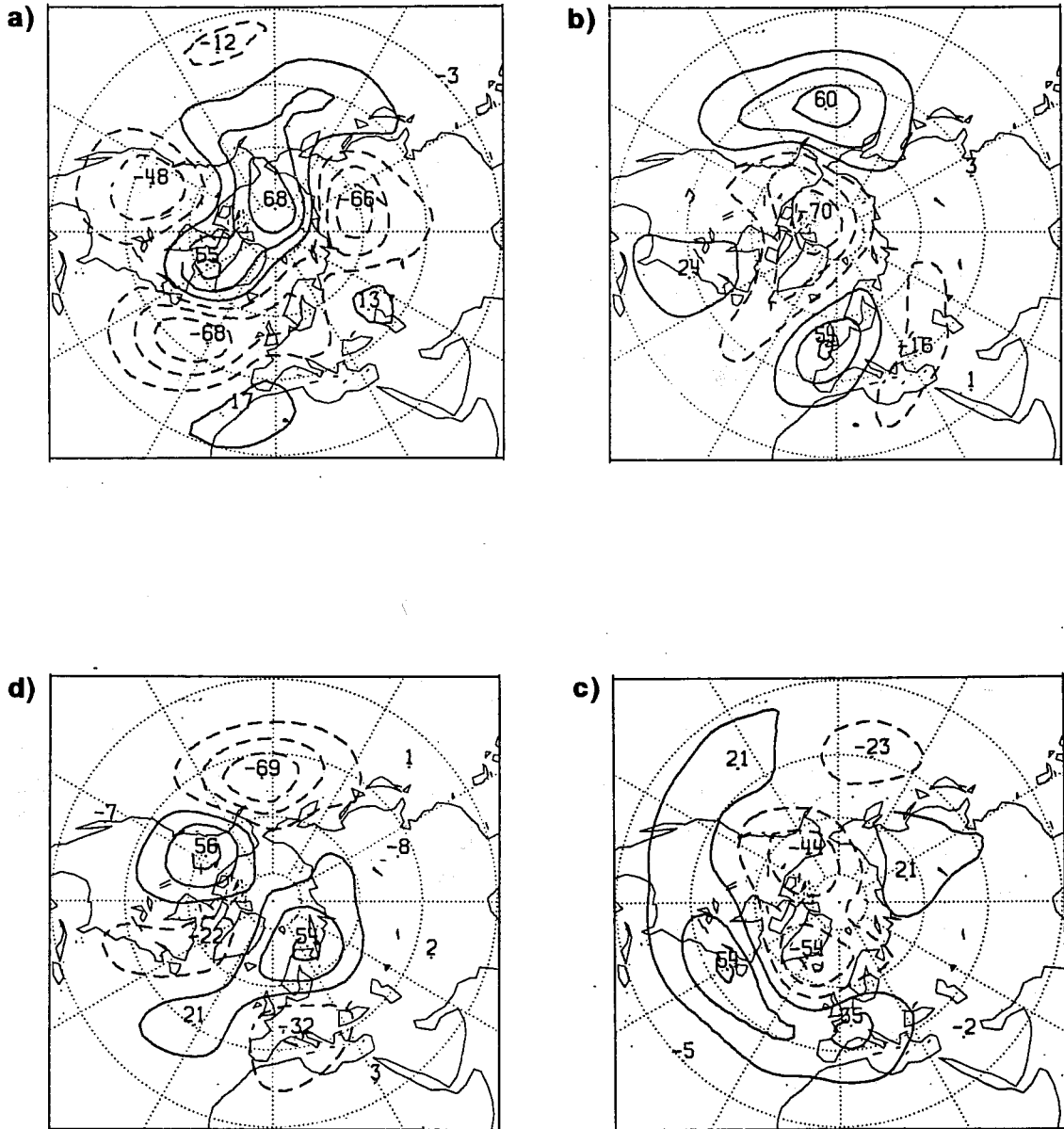
Fig. 5   Composite of extratropical 500mb geopotential height (m) formed by taking from the 700 winter fields, days where a) the coefficient of the second EOF of OLR was greater than one standard deviation. b) the coefficient of the first EOF of OLR was greater than one standard deviation. c) the coefficient of the second EOF of OLR was less than minus one standard deviation. d) the coefficient of the first EOF of OLR was less than minus one standard deviation. Contour interval 20 m.
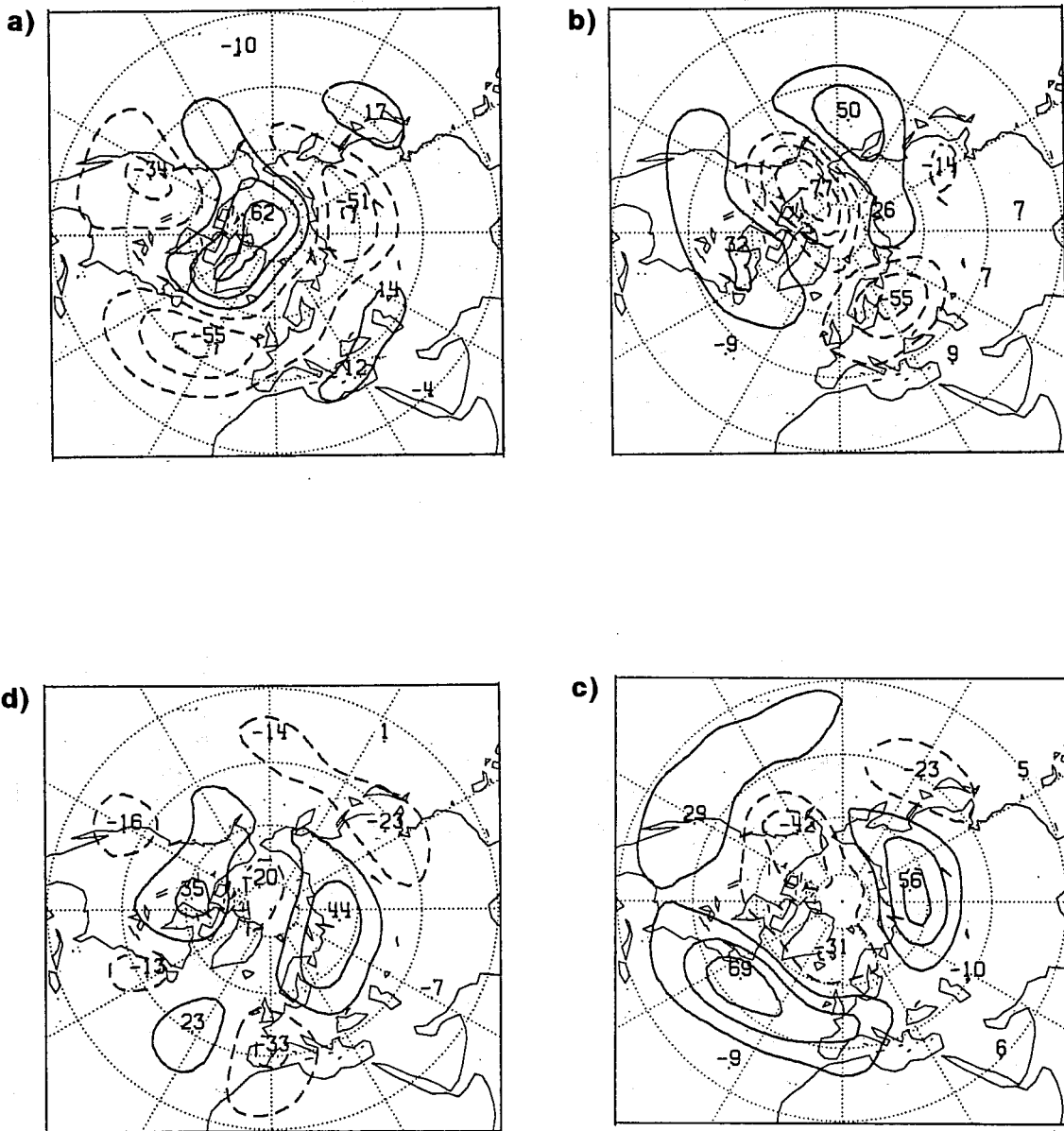
Fig. 6 Composite of extratropical 500mb geopotential height (m) formed by taking from the 700 winter fields days where, 12 days after a) the height field was part of the composite in Fig 5d. b) the height field was part of the composite in Fig 5a. c) the height field was part of the composite in Fig 5b. d) the height field was part of the composite in Fig 5c. Contour interval 20 m.
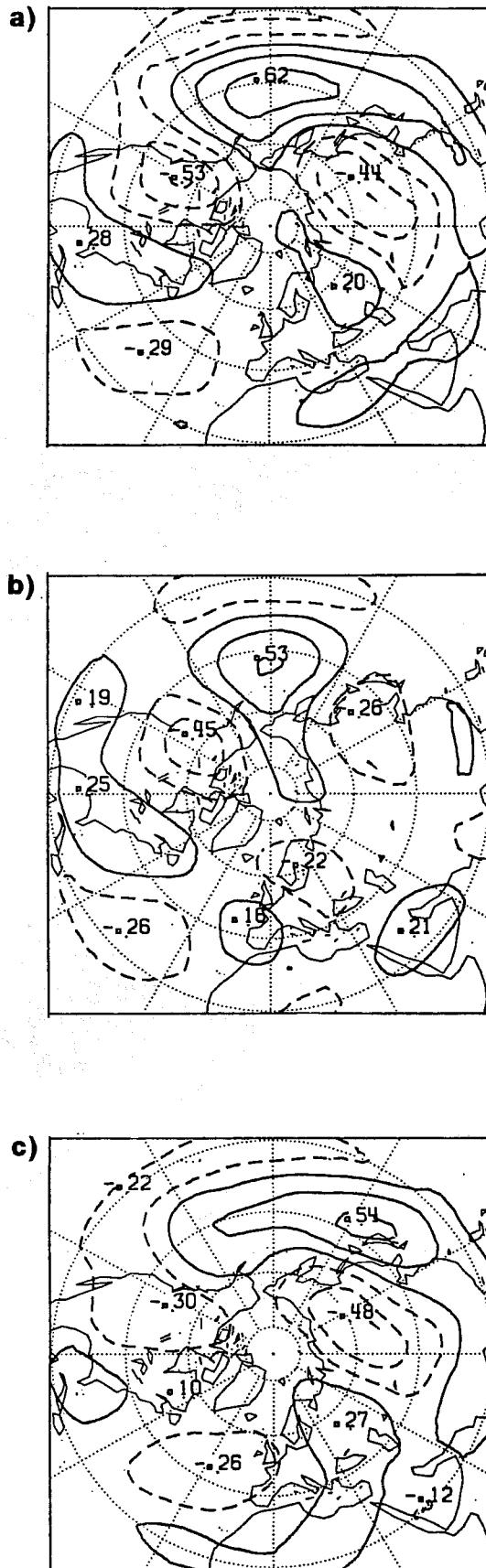
Fig. 7 Teleconnection maps showing the correlation between OLR averaged over the area 15-20N, 135-150E, and 500mb geopotential height at each gridpint in the northern hemisphere. (a) simultaneous correlation (b) when geopotential height lags OLR by 5 days. (c) when geopotential height leads OLR by 5 days. Contour interval 0.15, zero contour not shown.
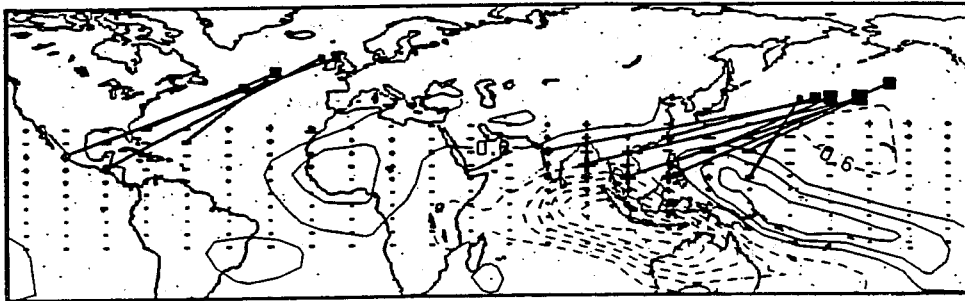
Fig. 8   Schematic illustration of the relationship between the location of the forcing region and the maximum midlatitude response excited from it. (From Simmons et al, 1983). Contours of the first EOF of OLR from the present study are superimposed.
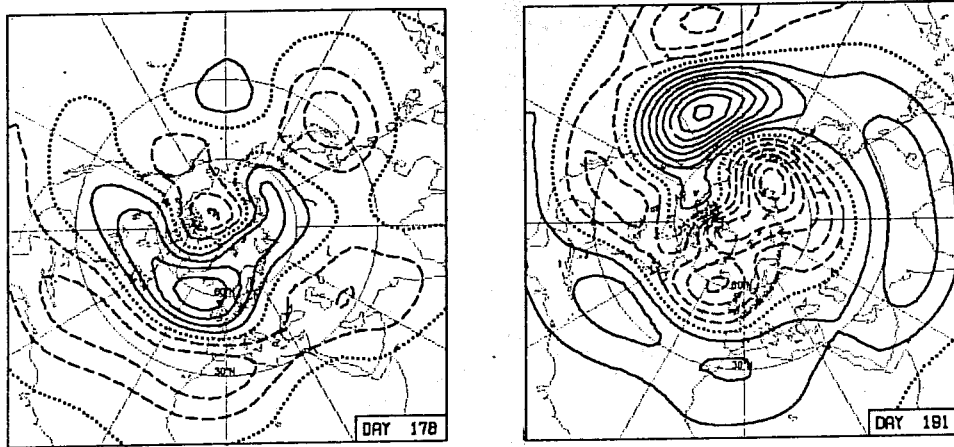
Fig. 9   Structure of the most unstable mode of a January 300mb basic state flow, shown as two phase-quadrature components (from Simmons et al, 1983)
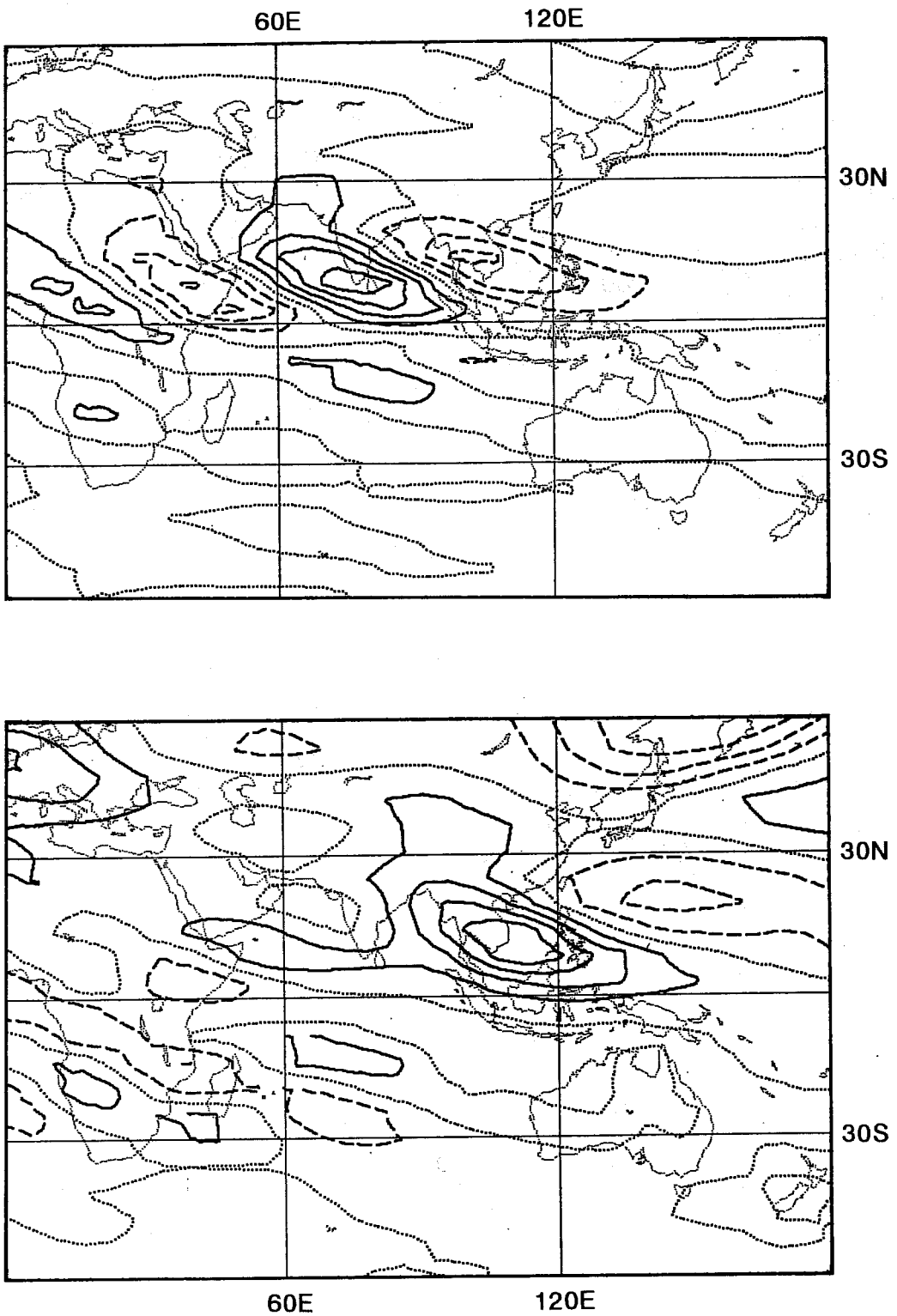
Fig. 10 Structure of the adjoint to the normal mode shown in Fig 9 (defined with respect to an energy inner product) shown as two phase-quadrature components. (Amplitude normalised).
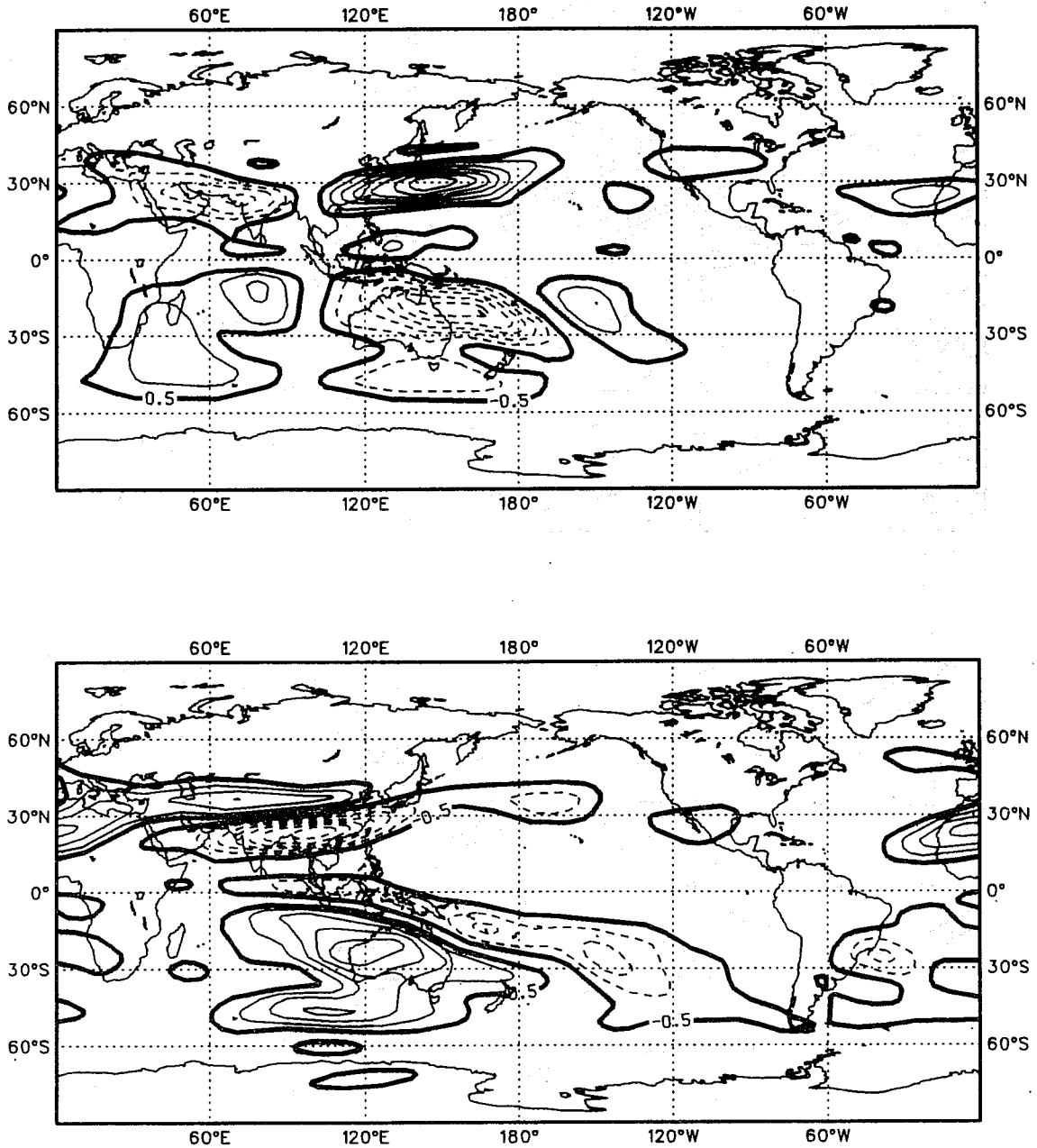
Fig. 11 Structure of the 48 day period vorticity forcing, shown as two phase quadrature components, derived from the first two EOFs of OLR as shown in Fig 1. Contour interval .5 x 10⁻³ sec⁻², zero contour not shown.
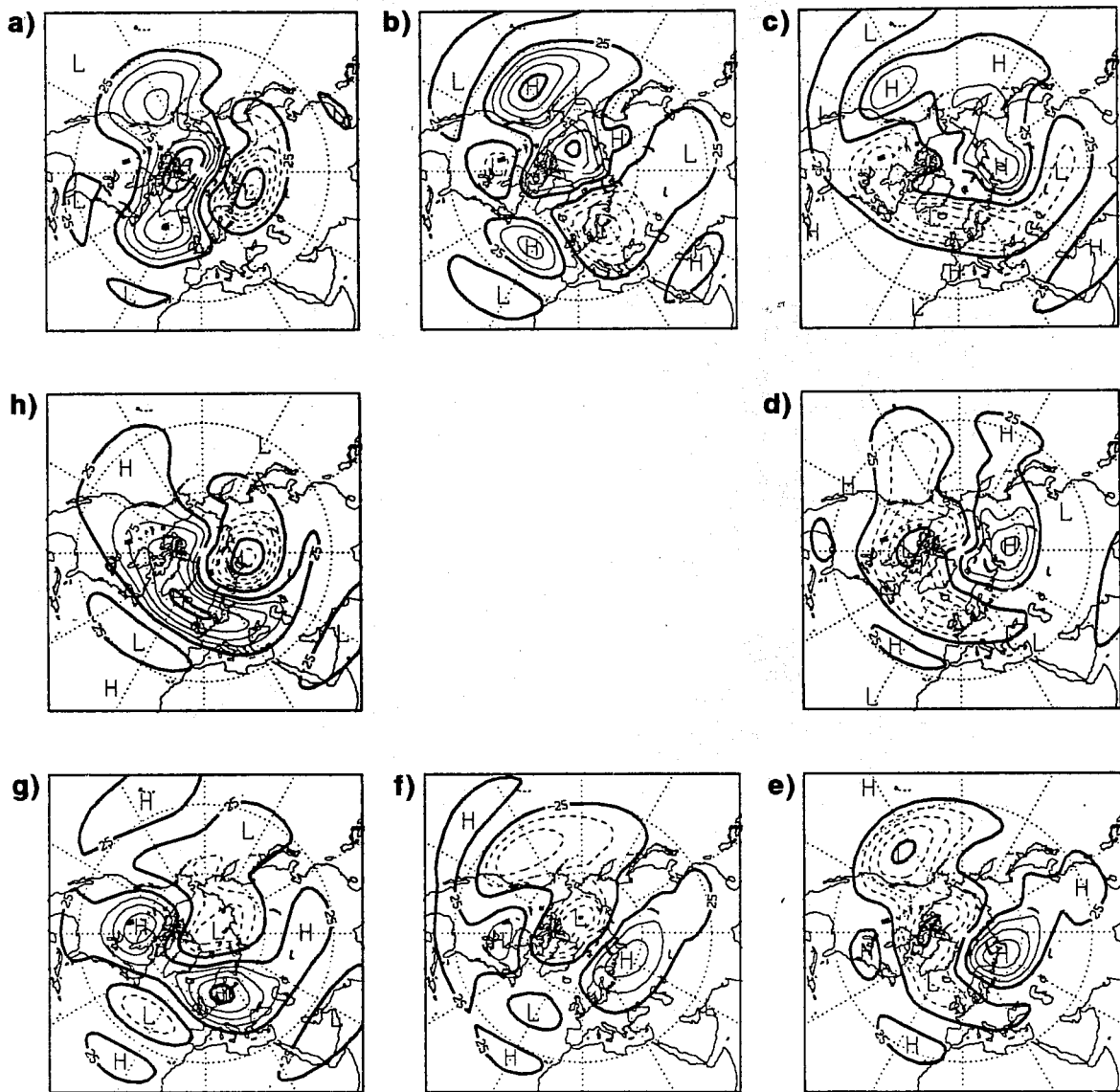
Fig. 12   Streamfunction response (multiplied by the Coriolis parameter) of a barotropic model with climatological January basic state and forcing given by Fig 11, integrated through 8 48-day cycles.   a)-h) 6-day mean composites over the eight cycles. Contour interval 25 m.

Days 1-5

Days 11-15

4 Dec 84
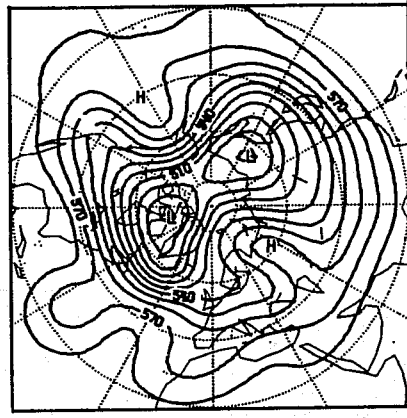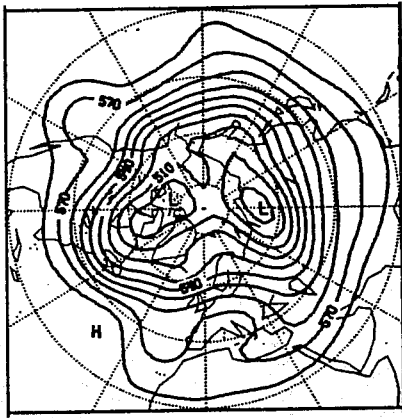
25 Dec 84
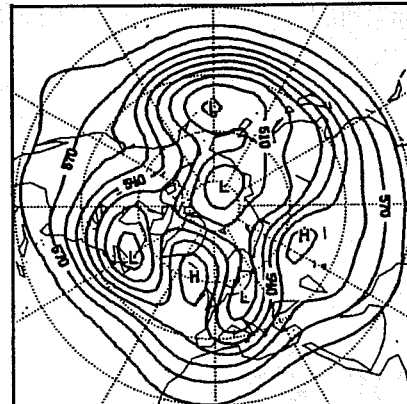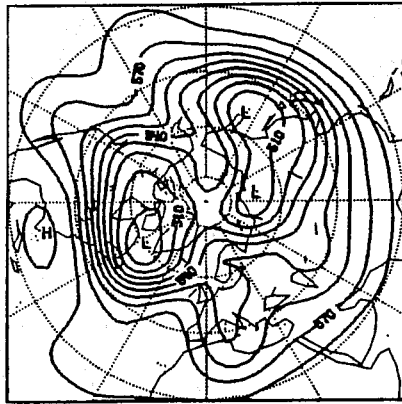
22 Jan 85
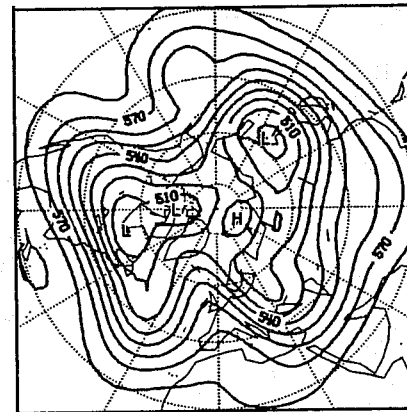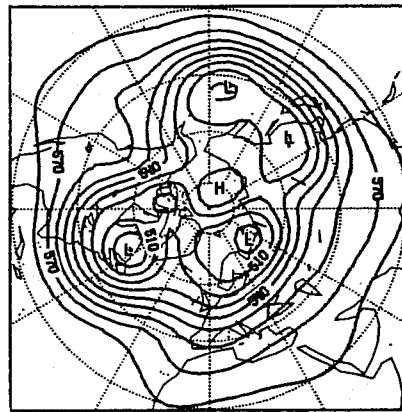
19 Jan 86
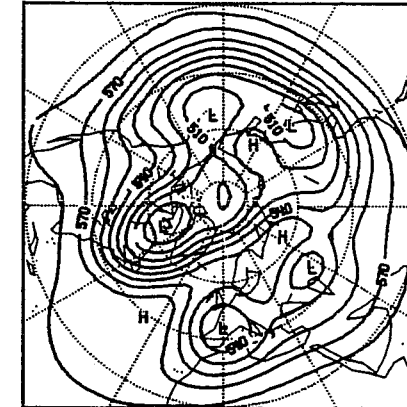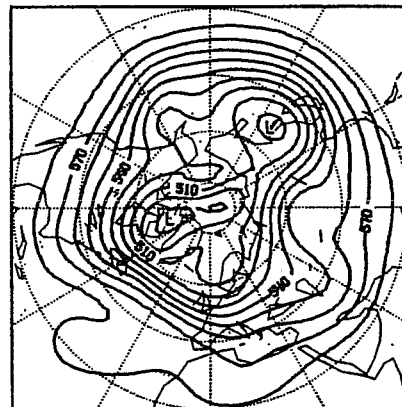
Fig. 13   Observed 5-day mean 500mb height for days 1-5 and 11-15   of each of the four
20-day periods chosen for study. Contour interval 10 dam.
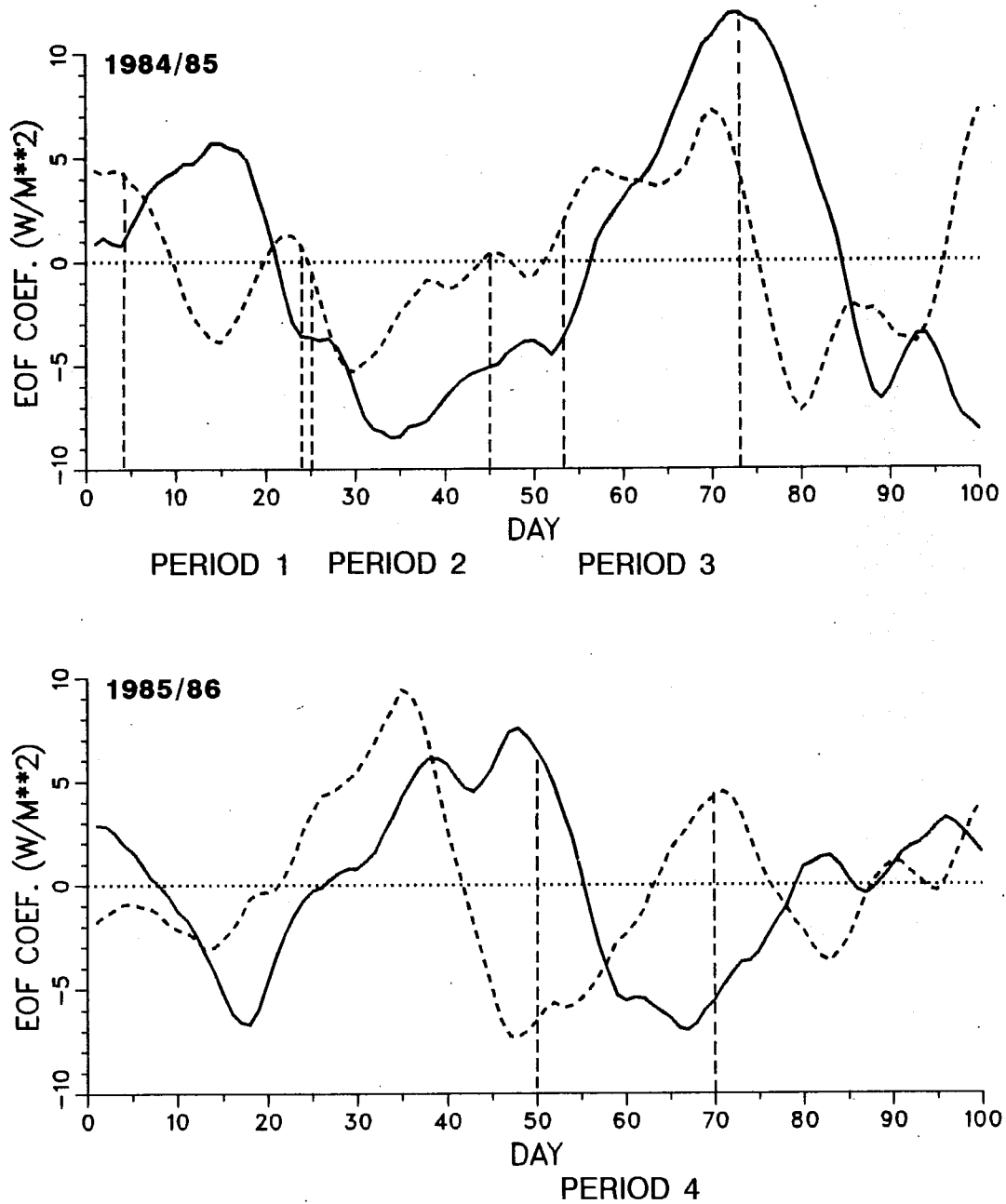
Fig. 14   Time series of first two EOF coefficients of OLR for the winters 1984/85 and
1985/86. Day one is the first of December. EOF1: solid line, EOF2: dashed line.
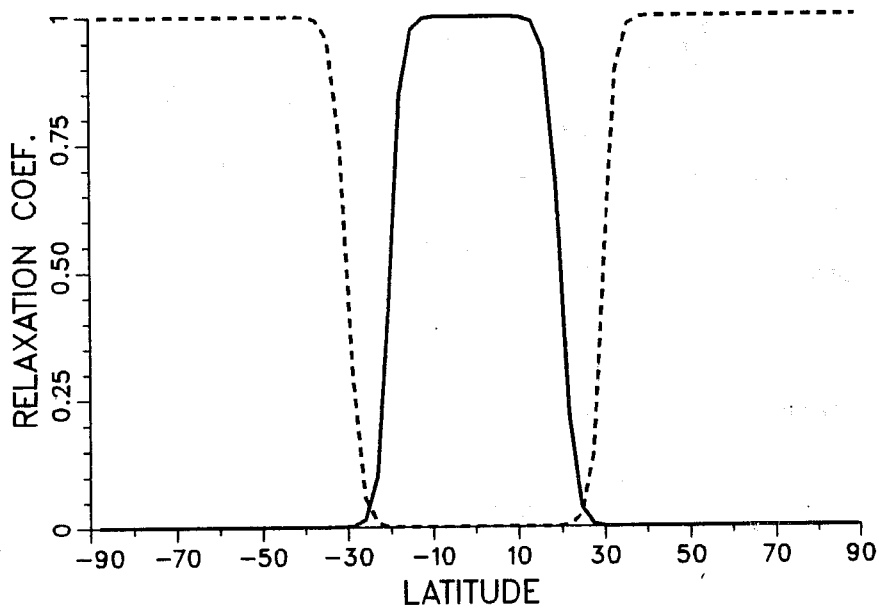
Fig. 15   Graphs showing the value of the relaxation coefficient (as a fraction of the maximum relaxation of (8hr)$^{-1}$) as a function of latitude for relaxation in the tropics (solid line), relaxation in the extratropics (dashed line).
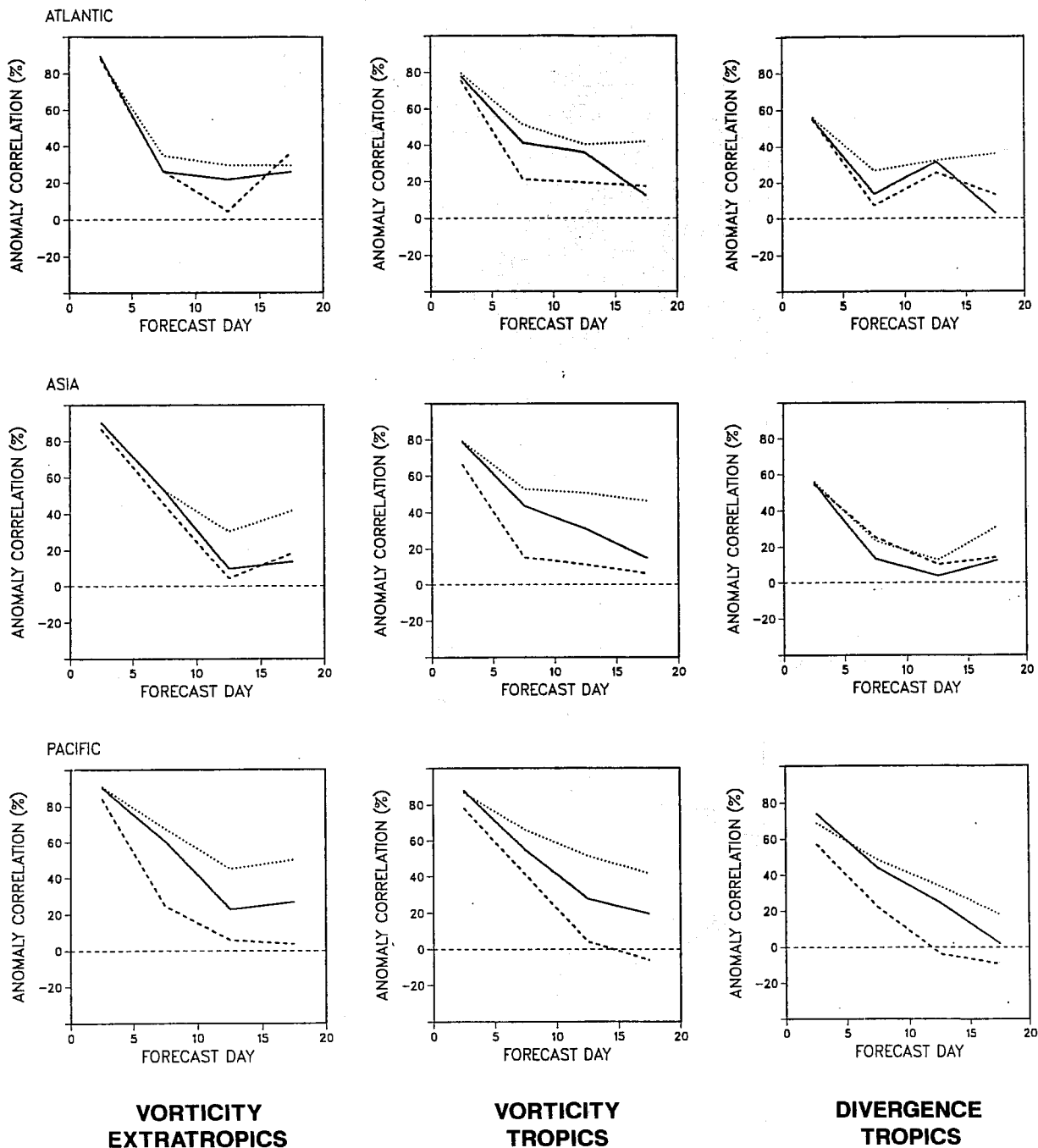
Fig. 16   Anomaly   correlation   coefficient   of   5-day   mean   200mb   vorticity,   and   divergence
fields   averaged   over   all   four   experiments.   The   left   hand   column   shows
extratropical   vorticity   scores;   the   middle   column   shows   tropical   vorticity
scores;   the   right   hand   column   shows   tropical   divergence   scores.   Scores
for   the   control   forecast   are   shown   as   solid   lines;   scores   for   the   experiments   with
relaxation   towards   the   analysis   are   shown   as   dotted   lines;   scores   for   the
experiments with relaxation towards initial conditions are shown as dashed lines.
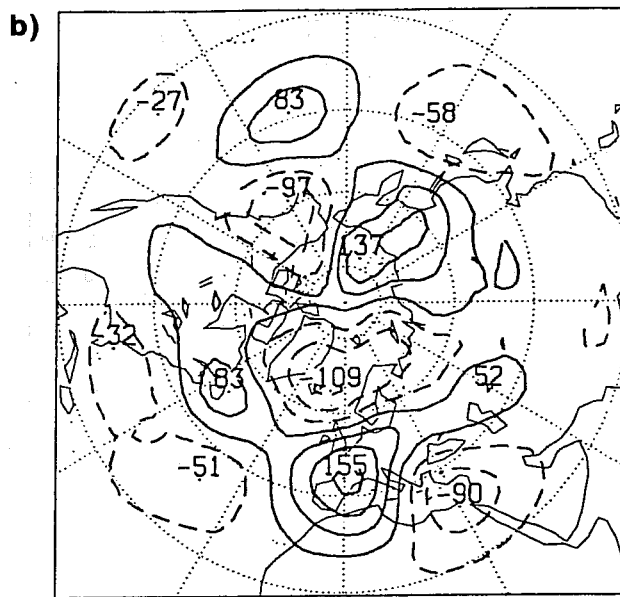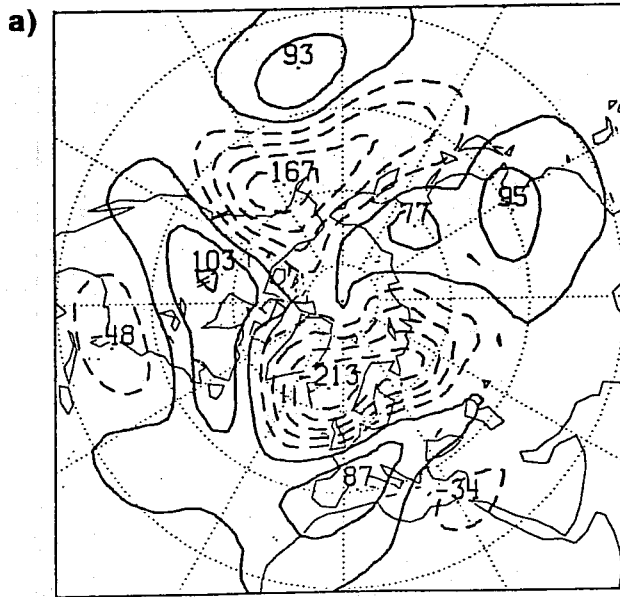
a)

b)

Fig. 17   'Systematic'   error   in   500mb height   for days   11-20 for   a) control forecasts   b)
integrations   with   tropics   relaxed   towards   analyses,   obtained   by   averaging
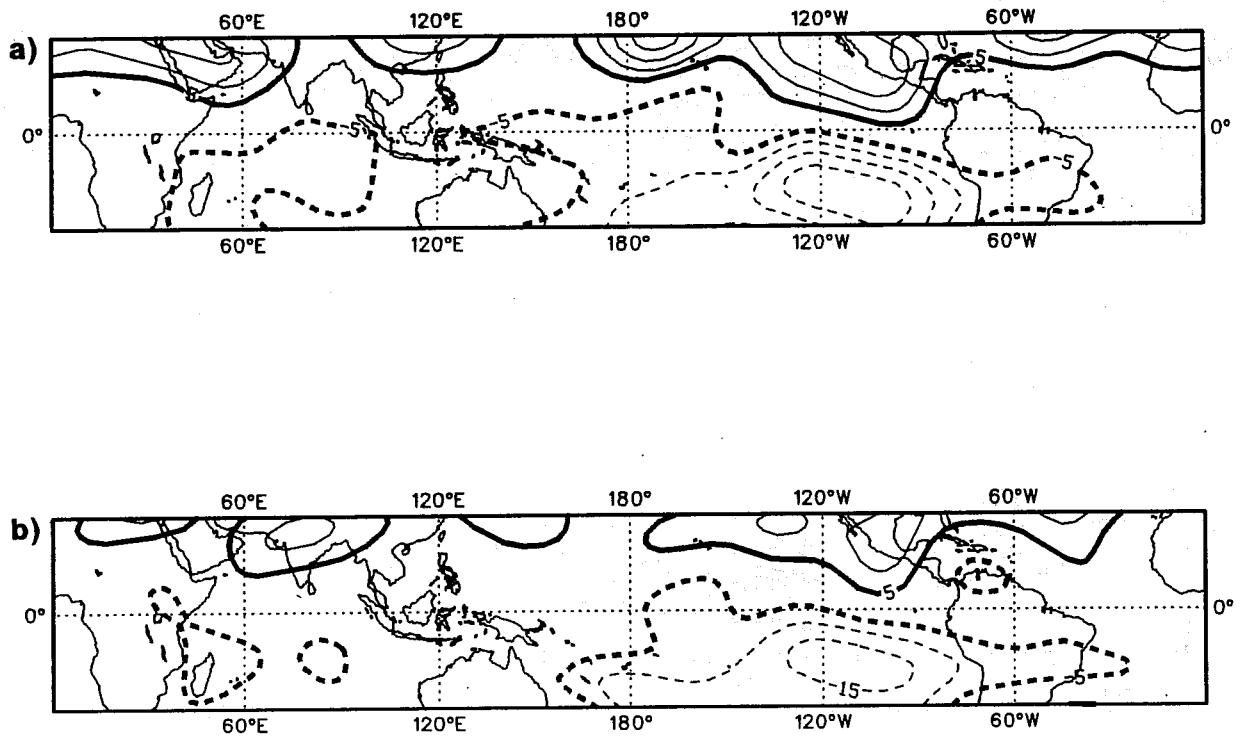the 4 respective forecast errors together. Contour interval 40 m.

Fig. 18 'Systematic' error in 200mb tropical streamfunction for days 11-20 for a) control forecasts b) integrations with extratropics relaxed towards analyses. Contour interval 5×10^{-6} m^2.sec^{-1}. A gradient of 1 contour interval in 10 degrees gives a speed of 5 m/sec.

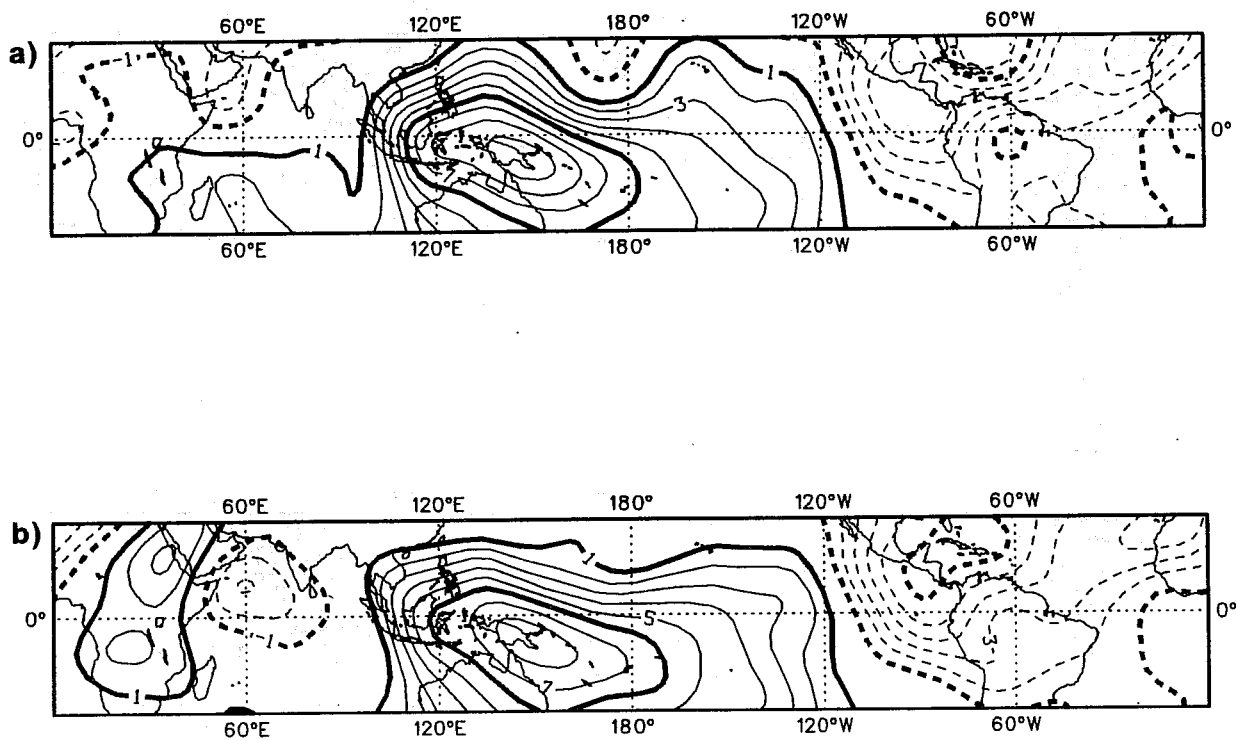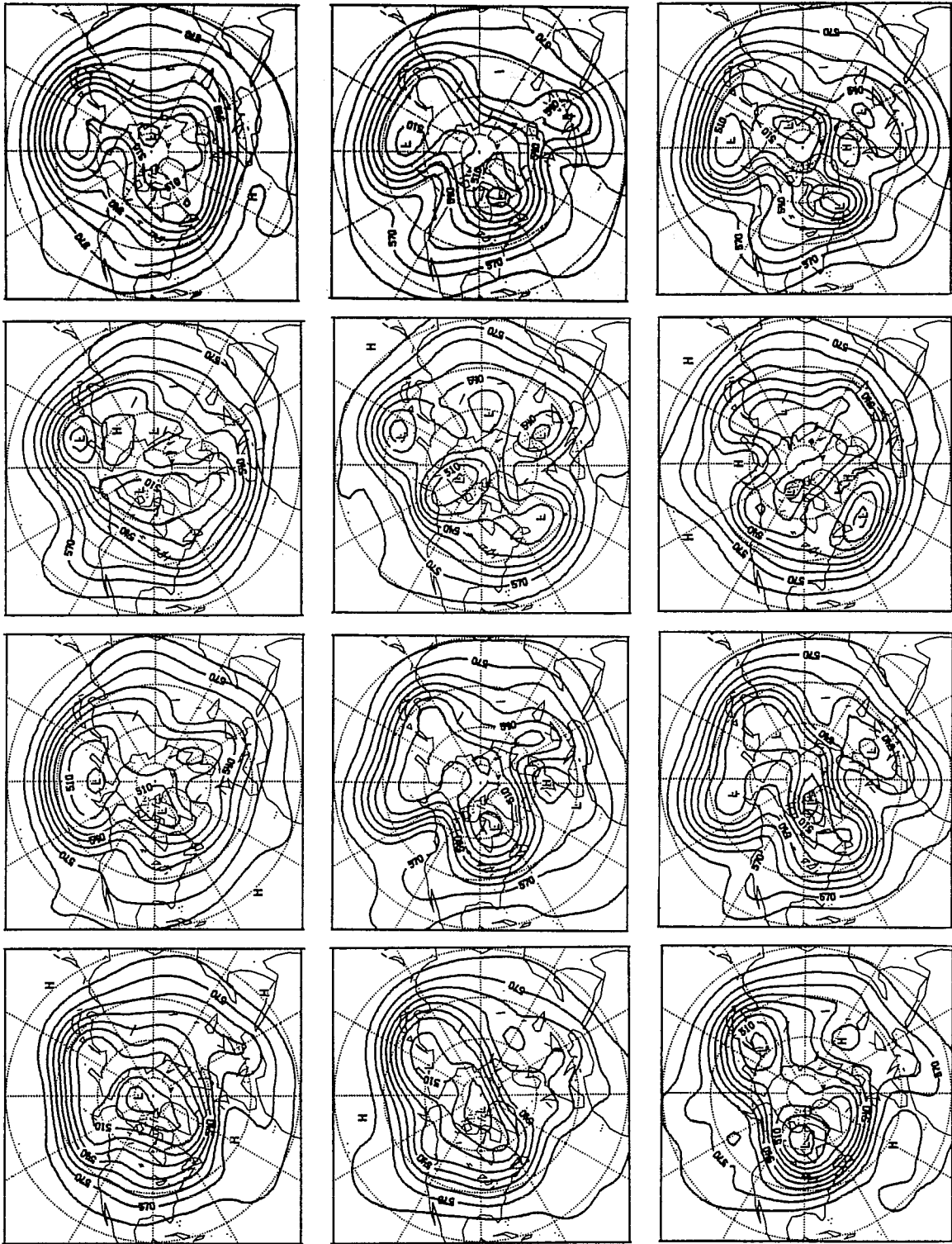Fig. 19   As Fig 18 but for 200mb tropical velocity potential. Contour interval 1x10⁻⁶ m².sec⁻¹. Dashed contours negative, solid contours positive, flow from low to high values. A gradient of 1 contour interval in 10 degrees gives 1 m/sec.

4 Dec 84   **25 Dec 84**   **22 Jan 85**   **19 Jan 86**

Fig. 20   Maps of 500mb height for day 16-20 of the control integration (top row), the integration with relaxed tropics (middle row), and the verifying analysis (bottom row), for each individual case.
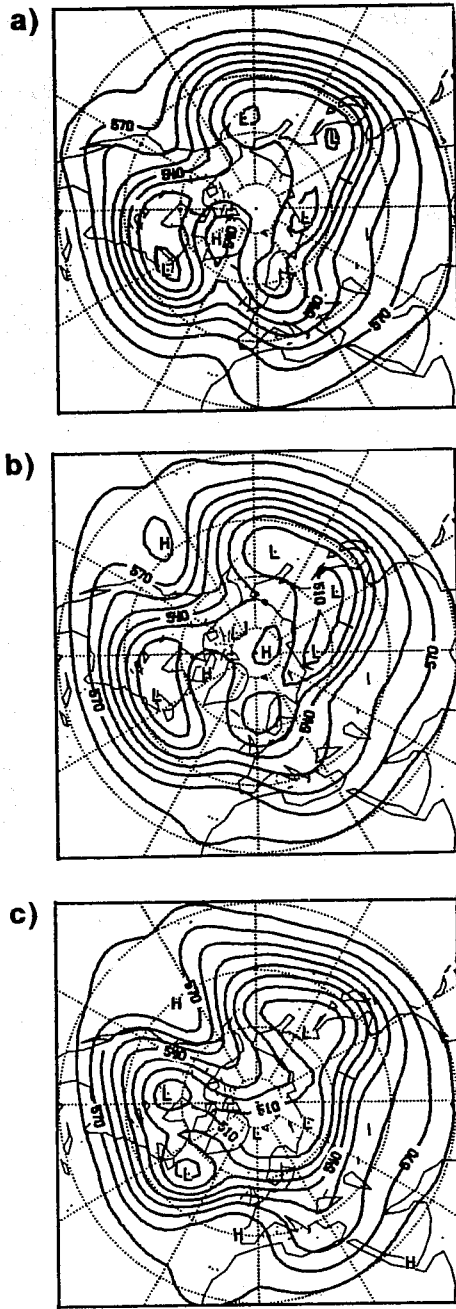
Fig. 21   Maps of 500mb height for days 6-10 of a) control integration,   b) integration with relaxed tropics, and c) verifying analysis for 22 January case.

16-20   11-15   6-10

Fig. 22 Difference maps of 500mb height for 22 January 1985 case. Left hand column: days 6-10. Middle column: days 11-15. Right hand column: days 16-20. Top row: experiment with relaxation towards verifying analysis in tropics minus experiment with relaxation towards initial analysis in tropics. Bottom row: difference between verifying analysis and verifying analysis for days 1-5. Contour interval 50 m.